JOURNAL OF NATURAL PRODUCTS

Article

pubs.acs.org/jnp

Absolute Configuration of Acremoxanthone C, a Potent Calmodulin Inhibitor from *Purpureocillium lilacinum*

Abraham Madariaga-Mazón,[†] Martín González-Andrade,[‡] María del Carmen González,[§] Anthony E. Glenn,[⊥] Carlos M. Cerda-García-Rojas,*[,∥] and Rachel Mata*[,†]

[†]Facultad de Química, Universidad Nacional Autónoma de México, México D.F., 04510, Mexico

[‡]Instituto Nacional de Medicina Genómica, Secretaría de Salud, México, D.F., 14610, Mexico

[§]Instituto de Biología, Universidad Nacional Autónoma de México, México D.F., 04510, Mexico

[⊥]Toxicology & Mycotoxin Research Unit, 950 College Station Road, USDA-ARS, Russell Research Center, Athens, Georgia 30605, United States

[∥]Departamento de Química, Centro de Investigación y de Estudios Avanzados del Instituto Politécnico Nacional, Apartado 14-740, México D.F., 07000, Mexico

Supporting Information

ABSTRACT: Bioassay-guided fractionation of an extract prepared from the culture medium and mycelium of *Purpureocillium lilacinum* allowed the isolation of two calmodulin (CaM) inhibitors, namely, acremoxanthone C (**1**) and acremonidin A (**2**). The absolute configuration of **1** was established as 2*R*, 3*R*, 1′*S*, 11′*S*, and 14′*R* through extensive NMR spectroscopy and molecular modeling calculations at the DFT B3LYP/DGDZVP level, which included the comparison between theoretical and experimental specific rotation, $^{3}J_{C,H}$, and $^{3}J_{H,H}$ values. Compounds **1** and **2** bind to the human calmodulin (*h*CaM) biosensor *h*CaM M124C-*mBBr*, with dissociation constants (K_d) of 18.25 and 19.40 nM, respectively, 70-fold higher than that of chlorpromazine (K_d = 1.24 μM), used as positive control. Docking analysis using AutoDock 4.2 predicted that **1** and **2** bind to CaM at a similar site to that which KAR-2 binds, which is unusual. Furthermore, a novel, sensible, and specific fluorescent biosensor of *h*CaM, i.e., *h*CaM T110C-*mBBr*, was constructed; this device is labeled at a site where classical inhibitors do not interact and was successfully applied to measure the interaction of **1** with CaM. This is the first report of xanthone−anthraquinone heterodimers in species of *Paecilomyces* or *Purpureocillium* genera.

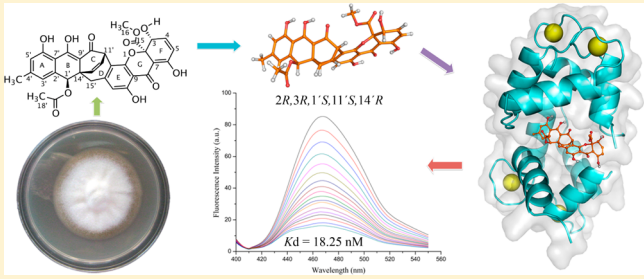

Purpureocillium lilacinum (Thom) Luangsa-ard, Houbraken, Hywel-Jones & Samson is a ubiquitous, saprobic filamentous fungus commonly isolated from soil, decaying vegetation, insects, nematodes, and other environments. This fungus is an emergent pathogen that causes severe human infections, but is used as an important biological control agent against nematodes.[1−4] A recent comparative study of a few clinical isolates of this fungus with strains isolated from soil, insects, and nematodes using 18S rRNA gene, internal transcribed spacer (ITS), and partial translation elongation factor 1-α (TEF) sequences revealed that *P. lilacinum* is not related to *Paecilomyces*. Therefore, a new genus named *Purpureocillium* was proposed for the fungus, and the new combination *Purpureocillium lilacinum* (Thom) Luangsa-ard, Houbraken, Hywel-Jones & Samson was made for this species.[1−4]

A few metabolites have been isolated from *P. lilacinum*, including the neutral peptides regarded as paecilotoxins[5,6] and the novel pyridone alkaloid paecilomide.[7] The peptides exhibited moderate antimicrobial properties and strong uncoupling activity against rat liver mitochondria,[5,6] while paecilomide was an inhibitor of acetylcholinesterase.[7]

In our continuous search for calmodulin (CaM) ligands from fungi,[8−12] we have now studied *P. lilacinum*, isolated from a soil sample of a cave in Juxtlahuaca, State of Guerrero, Mexico, and obtained two xanthone−anthraquinone heterodimers, namely, acremoxanthone C[13] (**1**) and acremonidin A[14] (**2**).

Calmodulin is a small (148 residues), acidic, and highly conserved protein, possessing homologous N- and C-terminal globular domains connected by a flexible central linker.[15] Each globular domain contains two Ca^{2+} binding sites of the helix−loop−helix (EF-hand) type.[16] Ca^{2+} binding to the protein induces the exposure of its hydrophobic patches, allowing binding to specific proteins and adopting a compact globular structure wrapped around its targets. Calmodulin interacts with many cellular targets to regulate their function, resulting in modulation of a large number of Ca^{2+}-dependent signal transduction processes including gene regulation, protein synthesis, ion channel function, cell motility, organelle tubulation, chemotaxis, and smooth muscle contraction, to

Received: March 22, 2013
Published: July 22, 2013

mention a few.[17] Several synthetic or natural occurring compounds also bind to CaM in different domains, modifying its physiological function. Some of these compounds are used as valuable tools to study CaM-mediated pathways or as pharmacological agents for treating chronic or degenerative diseases.[18,19] Thus, the discovery of new and more potent CaM inhibitors with a novel binding mode could lead to the discovery of new research tools or drugs with unique pharmacological properties.

Herein, we describe the isolation, absolute configuration, CaM binding properties, and docking studies of acremoxanthone A (**1**). Furthermore, a novel, sensible, and specific fluorescent biosensor of human CaM (*h*CaM T110C-*mBBr*), labeled at a site where classical inhibitors of the protein do not interact, was constructed and successfully applied to evaluate compounds **1** and **2**.

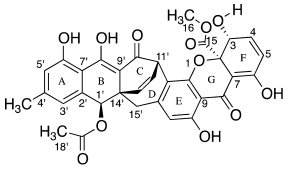

1

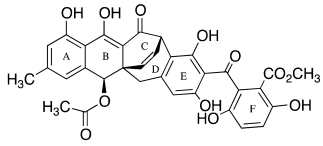

2

RESULTS AND DISCUSSION

An extract prepared from the culture medium and mycelium of *P. lilacinum* quenched the fluorescence of the CaM biosensor *h*CaM M124C-*mBBr*[20] by 50%, suggesting the presence of one or more CaM ligands. Reversed-phase liquid chromatography of the active extract allowed the isolation of two CaM ligands, acremoxanthone C (**1**) and acremonidin A (**2**). The structures of **1** and **2** were determined by spectroscopic and spectrometric analyses and comparison with reported data.[13,14] Acremoxanthone C (**1**) was recently isolated from an unidentified fungus of the Hypocreales order. The characterization of **1** was achieved by NMR analysis; the relative configuration at C-1′, C-14′, and C-11′ was designated on the basis of the ROESY experiment, which showed a correlation between the acetate C-18′ methyl group and H-13′.[13] All attempts to assign the absolute configuration at C-2 via the Mosher esters failed. In all cases, the G-ring opened under the basic conditions, yielding compound **2** and other minor products. Thus, the absolute configuration at C-2, C-3, C-1′, C-14′, and C-11′ could not be unambiguously established.

The affinity of **1** and **2** for CaM was assessed using the fluorescent biosensor *h*CaM M124C-*mBBr*; the fluorescence titration curves (λ_{ex} 381 nm; λ_{em} 415−550 nm) of *h*CaM M124C-*mBBr* were assembled as depicted in Figure 1. The results showed that **1** and **2** bind to the protein with dissociation constants (K_d) of 18.25 ± 3.01 and 19.40 ± 3.15 nM, respectively, in a stoichiometric ratio of 1:1. These values were consistent with their higher affinity (70-fold) to the protein than CPZ (K_d = 1.24 μM), a well-known classic CaM inhibitor used as positive control. Compounds **1**, **2**, and CPZ quenched the fluorescence of the biosensor with values of 47%, 48%, and 90%, respectively. The level of affinity to CaM of **1** and **2** is unusual, since most CaM antagonists bind to the protein with much lower affinity, usually in the micromolar range.

Considering the extraordinary affinity of **1** to CaM, we decided to complete its structural characterization by establishing its absolute configuration. Thus, molecular modeling calculations at the DFT B3LYP/DGDZVP level were undertaken[21,22] in order to determine the calculated specific rotation and $^3J_{C,H}$ and $^3J_{H,H}$ values for all possible diastereoisomers of **1**. The calculated data were next compared with the experimental parameters.

Sixteen stereoisomers, in two enantiomeric series, are conceivable for **1**, since the bridgehead carbons (C-11′ and C-14′) can only be β- or α- oriented. The structure for each member of the β-series was built and minimized using the Spartan'02 software (Figures S1 and S2). For all diastereoisomers a conformational search was performed applying the molecular mechanics Monte Carlo protocol, followed by geometry optimization for each generated conformer using DFT calculations at the B3LYP/DGDZVP level, as implemented in the Gaussian 09 software. The optical rotation calculations were performed for each fully minimized conformer within an energy window of 0−3 kcal/mol (Tables S1−

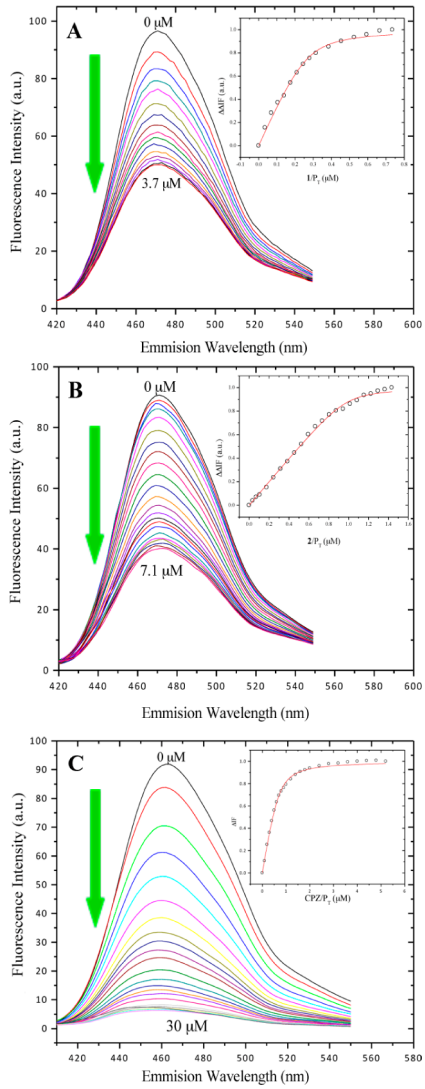

Figure 1. Fluorescence spectra and titration curves of *h*CaM M124C-*mBBr* (5 μM) to saturation ion Ca^{2+} (10 mM). (A) **1**, 18.25 nM; (B) **2**, 19.40 nM; and (C) CPZ, 1.24 μM. Buffer was 10 mM potassium acetate (pH 5.1) at 37 °C. Samples were excited at 381 nm, and emission spectra recorded from 415 to 550 nm. The absolute changes of maximal fluorescence emission were corrected for light-scattering effects and plotted against the ligands to total protein ratio (insets).

dx.doi.org/10.1021/np4002477 | J. Nat. Prod. 2013, 76, 1454−1460

S8). Once the results were Boltzmann-weighted, it was found that regardless of the absolute configuration of the C-2, C-3, and C-1′ stereogenic centers, the eight isomers (**A**–**H**) possessing the bridgehead carbon atoms β-oriented (11′*S*,14′*R*) had positive $[\alpha]_D$ values, while those α-oriented (11′*R*,14′*S*) had negative values (Table S9). In this regard, all reported xanthone–anthraquinone heterodimers of the acremoxanthone series possess a β-oriented C-11′–C-14′ bridgehead and positive $[\alpha]_D$ values. Thus, the biosynthesis of this type of compound seems to be restricted to the β-oriented C-11′–C-14′ bridgehead isomers.[14,23–25] The calculated specific rotation data of those isomers having positive values were compared with the experimental value recorded for **1**. According to the results in Table 1, the $[\alpha]_D$ value calculated for isomer **A** matched best with the experimental value for acremoxanthone C (**1**). This finding also implied that the absolute configurations at C-2, C-3, C-1′, C-11′, and C-14′ were *R*, *R*, *S*, *S*, and *R*, respectively (Figure 2). Furthermore, the strong correlations between closely located H-1′ and H-15′α (distance = 2.86 Å) and H-15′β (distance = 2.44 Å) in the NOESY spectrum of **1** provided additional evidence for the *S* configuration at C-1′, ruling out stereoisomers **E**–**H**.

Table 1. DFT-Calculated $[\alpha]_D$ Values[a] for the Eight Diastereoisomers of Acremoxanthone C (1) Possessing the Bridgehead Carbon Atoms β-Oriented

stereoisomer	absolute configuration	contributing conformers[b]	$[\alpha]_D$[c]	difference[d]
A	2*R*, 3*R*, 1′*S*, 11′*S*, 14′*R*	5	+467.22	12.9
B	2*R*, 3*S*, 1′*S*, 11′*S*, 14′*R*	5	+715.91	33.3
C	2*S*, 3*R*, 1′*S*, 11′*S*, 14′*R*	5	+638.69	18.9
D	2*S*, 3*S*, 1′*S*, 11′*S*, 14′*R*	4	+680.79	26.8
E	2*R*, 3*R*, 1′*R*, 11′*S*, 14′*R*	5	+425.40	20.8
F	2*R*, 3*S*, 1′*R*, 11′*S*, 14′*R*	5	+716.34	33.4
G	2*S*, 3*R*, 1′*R*, 11′*S*, 14′*R*	2	+446.56	16.8
H	2*S*, 3*S*, 1′*R*, 11′*S*, 14′*R*	3	+624.79	16.4

[a]DFT B3LYP/DGDZVP $[\alpha]_D$ values in degrees [dm g/cm^3]$^{-1}$. [b]Lowest free energy conformers whose contribution is approximately 99%. [c]Calculated with the equation $\sum_i [\alpha]_D^i \times P^i$, where $[\alpha]_D^i$ is the theoretical $[\alpha]_D$ value and P^i is the population for the *i*th conformer. [d]In percentage, calculated with the equation $|[([\alpha]_D^i/[\alpha]_D^o) \times 100] - 100|$, where $[\alpha]_D^i$ is the theoretical Boltzmann-weighted value for the corresponding isomer, and $[\alpha]_D^o$ is the experimentally observed value of $[\alpha]_D$ for **1** (+537.0).

To reinforce the proposed stereochemical assignment for acremoxanthone A (**1**), a selection of experimental $^3J_{C,H}$ and $^3J_{H,H}$ coupling constants were compared with the theoretical values obtained by DFT calculations, also at the B3LYP/DGDZVP level of theory. This approach was selected due to the close correlation between the $^3J_{C,H}$ or $^3J_{H,H}$ coupling constants and the corresponding ^{1}H–C–C–^{13}C or ^{1}H–C–C–^{1}H dihedral angles.[22] These values in combination with the pertinent molecular models provide accurate stereochemical information. Thus, experimental values for $^3J_{C,H}$ ($^3J_{C\text{-}7,H\text{-}3}$, $^3J_{C\text{-}7,H\text{-}5}$, and $^3J_{C\text{-}15,H\text{-}3}$) and $^3J_{H,H}$ ($^3J_{H\text{-}3,H\text{-}4}$) were measured in proton-coupled ^{13}C and ^{1}H NMR spectra, respectively. The comparative analysis was performed only for stereoisomers **A**–**D**, which possessed a β-oriented C-11′–C-14′ bridgehead and the appropriate distance between H-1′ and H-15′α to observe an interaction in the NOESY spectrum. Once more, the best correlation between the theoretical and experimental values (Table 2) was observed for stereoisomer **A** (2*R*,3*R*,1′*S*,11′*S*,14′*R*), ruling out structures **B**–**D** (Figure S1) for acremoxanthone C (**1**). The Boltzmann-averaged $^3J_{C\text{-}7,H\text{-}3}$, $^3J_{C\text{-}15,H\text{-}3}$, and $^3J_{H\text{-}3,H\text{-}4}$ values for structure **A** were significantly closer to the experimental values than those for structures **B**–**D**. Thus, in the proton-coupled ^{13}C NMR spectrum of **1**, C-7 appeared as a broad doublet with $^3J_{C\text{-}7,H\text{-}3} \approx 1.5$ (measured at $W_{1/2}$) and $^3J_{C\text{-}7,H\text{-}5} = 3.9$ Hz, and the carbonyl carbon (C-15) was observed as a double quartet with $^3J_{C\text{-}15,H\text{-}3} = 7.6$ Hz and $^3J_{C\text{-}15,H\text{-}16} = 3.3$ Hz, in agreement with the calculated values for structure **A**. In addition, the $^3J_{H\text{-}3,H\text{-}4}$ value of 2.1 Hz observed in the ^{1}H NMR spectrum of **1** provided further evidence in favor of stereostructure **A**, whose theoretical $^3J_{H\text{-}3,H\text{-}4}$ value was 2.5 Hz. In the case of stereostructures **B** and **C** the calculated $^3J_{H\text{-}3,H\text{-}4}$ values were 6.0 and 6.2 Hz, with RMSD values of 15.21 and 16.81, respectively, demonstrating a different geometry in the H-3–C-3–C-4–H-4 dihedral fragment. In addition, the large difference between the experimental $^3J_{C\text{-}15,H\text{-}3} = 7.6$ Hz and calculated values for stereoisomers **B** and **C** ($^3J_{C\text{-}15,H\text{-}3} = 3.3$ Hz and $^3J_{C\text{-}15,H\text{-}3} = 3.2$ Hz, respectively) as well as the larger difference between experimental and theoretical $^3J_{C\text{-}15,H\text{-}3} = 9.2$ Hz for stereoisomer **D** strengthened the selection of **A** as the structure for acremoxanthone C (**1**).

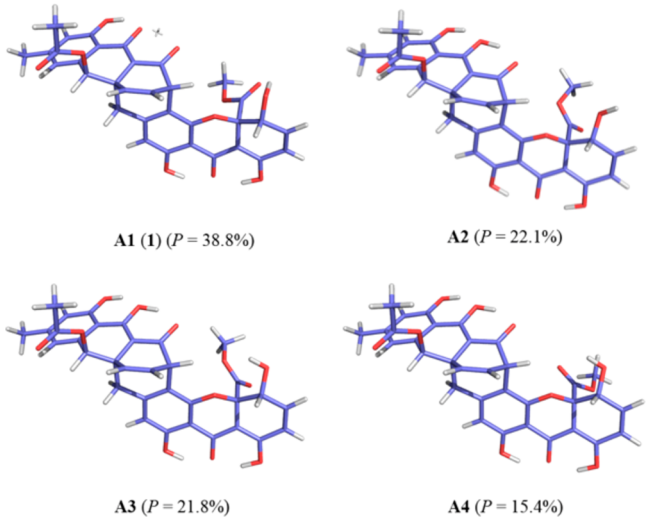

Figure 2. The most relevant DFT conformers of acremoxanthone C (**1**) accounting for 98.1% of the conformational population.

In order to the predict the binding site to CaM of **1** and **2**, a theoretical molecular study of docking was undertaken using the program AutoDock 4.2.[26] The cocrystallized structure of CaM with TFP was used (PDB code 1A29). The docking of **1** and **2** with the cocrystallized structure of CaM-TFP showed a nonclassical interaction; that is, the binding pocket was different from that for CPZ and TFP, which occupy one or more protein domains, respectively. The predicted K_i's were 406.9 and 367.6 nM, respectively. The predicted binding site for **1** and **2**, however, was similar to that of KAR-2, a vinblastine-derived antitumoral agent[27] that binds to CaM in a pocket between the N- and C-terminal globular domains like **1** and **2** theoretically do. KAR-2, **1**, and **2** seem to interact with

dx.doi.org/10.1021/np4002477 | J. Nat. Prod. 2013, 76, 1454–1460

Table 2. Comparison between Selected Experimental[a] and DFT-Calculated[b] $^{1}H-^{13}C$ and $^{1}H-^{1}H$ Couplings for Diastereoisomers A–D of Acremoxanthone C (1)

dihedral fragment X–C–C–Y	exp $^{3}J_{X,Y}$[a]	calcd[a] $^{3}J_{X,Y}$[b] for **A** (MSE)[c]	calcd[a] $^{3}J_{X,Y}$[b] for **B** (MSE)[c]	calcd[a] $^{3}J_{X,Y}$[b] for **C** (MSE)[c]	calcd[a] $^{3}J_{X,Y}$[b] for **D** (MSE)[c]
C-7–C-2–C-3–H-3	1.5	2.0 (0.25)	4.9 (11.56)	4.9 (11.56)	2.1 (0.36)
C-15–C-2–C-3–H-3	7.6	8.4 (0.64)	3.3 (18.49)	3.2 (19.36)	9.2 (2.56)
H-3–C-3–C-4–H-4	2.1	2.5 (0.16)	6.0 (15.21)	6.2 (16.81)	3.1 (1.0)
	RMSD[d]	0.59	3.88	3.99	1.14

[a]In Hz measured from the proton-coupled ^{13}C NMR or ^{1}H NMR spectra of **1** in $CDCl_3$. [b]Calculated from the B3LYP/DGDZVP-optimized structures and Boltzmann-averaged with the equation $\sum_i J^i \times P^i$, where J^i is the coupling constant value for each conformer and P^i is the population for the ith conformer. [c]Mean-squared error calculated with the equation $(J_e - J_c)^2$, where J_e is the coupling constant value measured from the experimental spectra and J_c is the calculated constant value. [d]Root-mean-square deviation, calculated from the equation $\sum_i (\mathrm{MSE})_i/n$, where MSE_i is the mean-squared error for each coupling constant and n is the total coupling constants to compare.

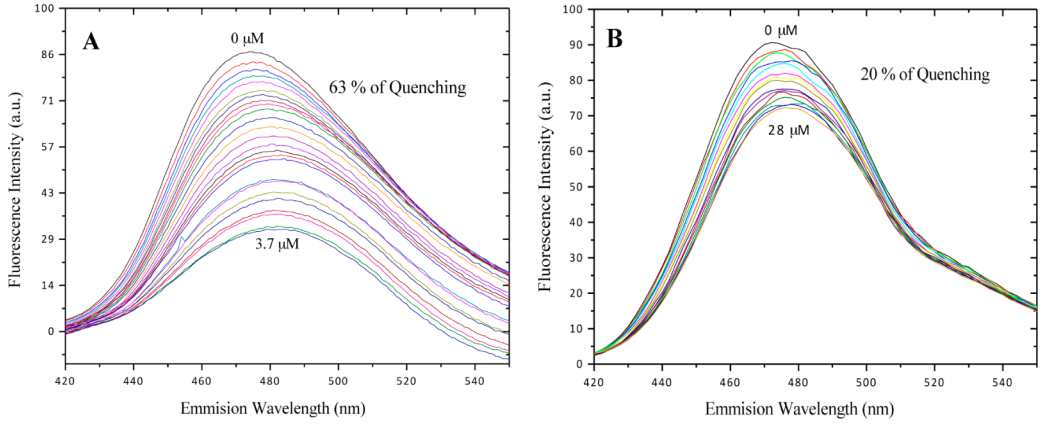

Figure 3. Fluorescence spectra of *h*CaM T110C-*mBBr* (5 μM; Ca^{2+} 10 mM) to saturation. (A) **1**, 63% of quenching. (B) CPZ, 20% of quenching. Buffer was 10 mM potassium acetate (pH 5.1) at 37 °C. Samples were excited at 381 nm, and emission spectra recorded from 415 to 550 nm.

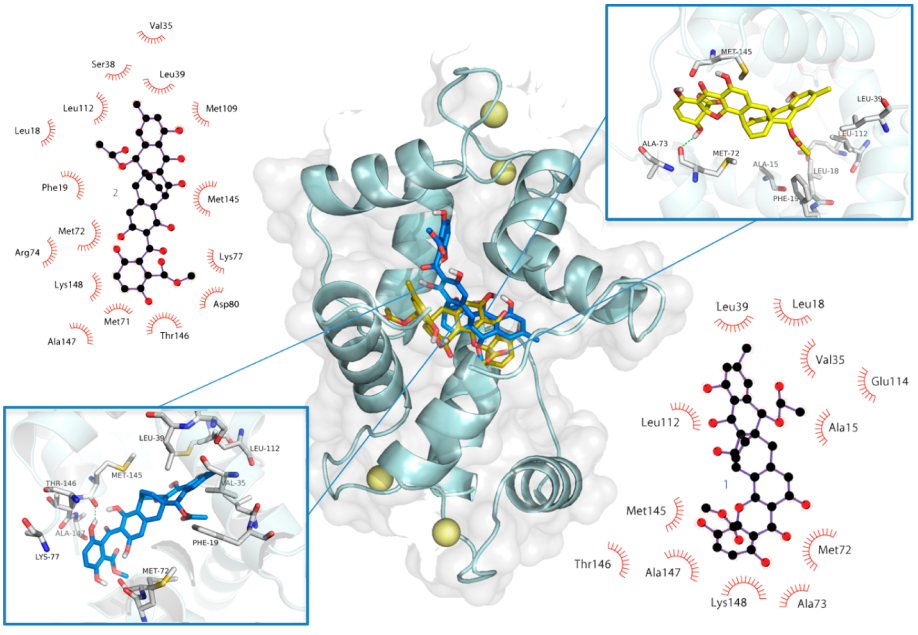

Figure 4. Structural model of CaM complexes represented in pale blue cartoon. The central panel shows the interaction of **1** (yellow sticks) and **2** (blue sticks) with CaM, using the crystallographic structure of the CaM (PDB code 1XA5). Details about the binding model of **1** and **2**, the amino acids involved in the interaction (white sticks) with the ligand, and hydrogen bonds (green dashed lines) are shown in the right and left panel, respectively. This figure was prepared using LigPlot and PyMOL.

several common amino acid residues, mainly hydrophobic, including Phe19, Ala15, Val35, Leu39, Gln41, Phe68, Ala73, Phe92, Met109, Leu112, Glu114, and Thr146; in addition, **1** forms a hydrogen bond between 3-OH and Met72 (distance = 1.9 Å), and **2** forms a similar interaction between 3-OH and Met145 (distance = 3.8 Å). Both types of interactions (hydrophobic and hydrogen bonds) play an important role in the stabilization of the protein–ligand complex (Figure 4). A docking study using the CaM-KAR-2 crystallized structure (PDB 1XA5) confirmed this supposition (Figure S3).

dx.doi.org/10.1021/np4002477 | *J. Nat. Prod.* 2013, 76, 1454–1460

Next, the affinity of **1** to CaM was measured with the newly designed *h*CaMT110C-*mBBr*, which was conceived for detecting nonclassical inhibitors of CaM. Device *h*CaMT110C-*mBBr* was generated following a conventional strategy that comprised site-directed mutagenesis for replacing the strategic residues Thr110 by Cys, followed by specific labeling of the thiol-reactive group with the fluorophore *mBBr*. This position was selected for labeling considering that residue 110 of CaM is in an accessible surface area (ASA = 50.17 Å^2) in the α-helix structure of CaM far from the binding site of classical inhibitors, and it is not involved in Ca^{2+} binding. The quantum efficiency of the *h*CaM T110C-*mBBr* device was ϕ = 0.303. Next, fluorescence titration curves with *h*CaM T110C-*mBBr* were constructed with saturating concentrations of **1** and CPZ (3.1 and 7.1 μM) in the presence of Ca^{2+} (10 mM). The results indicated that the fluorescence quenching is about 63% and 20% for **1** and CPZ, respectively. Furthermore, a shift of fluorescence maximum to higher wavelengths (red-shift) is observed for compound **1**. The higher percentage of quenching and the fluorescence maximum displacement caused by **1**, in comparison with CPZ, revealed that it binds to the protein in a different site than classical inhibitors.[28] The last set of results provided experimental support concerning the unusual binding site of **1** to CaM as predicted by the docking study. Ligands that interact with a novel binding domain on CaM might not inhibit most of the modulatory properties of CaM. For example, Horváth et al. demonstrated that the drug KAR-2 interacted with a novel drug-binding domain on CaM, allowing the protein to interrelate with most of its physiological targets. Furthermore, they concluded that this feature confers to KAR-2 its specificity and lack of significant toxic side effects.[19]

In summary, compounds **1** and **2** interact with CaM with higher affinity than CPZ, which is a classical inhibitor of the protein. The differences in quenching and the fluorescence maximum displacement caused by **1**, in comparison with CPZ, as detected by the newly designed *h*CaM T110C-*mBBr*, revealed that it might bind to the protein in a different site than classical inhibitors. Indeed, docking studies predicted that the binding site of **1** and **2** is unusual, different from that of classical inhibitors, but similar to that of KAR-2. Thus, *h*CaM T110C-*mBBr* can efficiently detect nonclassical inhibitors of CaM, while *h*CaM M124C-*mBBr* is an efficient device for quickly identifying in a sensitive and reliable manner both classical and nonclassical ligands.[12,24,29,12,30,31] This is the first report of xanthone−anthraquinone heterodimers in species of *Paecilomyces* or *Purpureocillium* genera.

EXPERIMENTAL SECTION

General Experimental Procedures. IR spectra were acquired using KBr disks in a Perkin-Elmer FT 59913 spectrophotometer. UV spectra were taken on a Shimadzu 160 UV spectrometer in $CHCl_3$ solution. The experimental optical rotations at the sodium D-line wavelength of pure compounds were recorded in $CHCl_3$ solution on a Perkin-Elmer 243 polarimeter at 23 °C. NMR spectra, including NOE differential, COSY, HMBC, and HSQC experiments, were recorded in $CDCl_3$ or methanol-d_4 on a Varian Unity Plus 500 spectrometer or on a Bruker DMX500 spectrometer operating at either 500 MHz (^{1}H) or 125 MHz (^{13}C), using TMS as an internal standard. RP-HPLC was carried out with a Waters HPLC instrument equipped with a Waters 996 UV photodiode array detector (900) set at 247/365 nm, using a PurospherSTAR RP-18e column (4.6 mm × 250 mm) and a gradient system starting with 50% MeCN in water, to 80% MeCN in 15 min, and 100% MeCN over 30 min, at a flow rate of 3.0 mL/min. Control of equipment, data acquisition and processing, and management of chromatographic information were performed by the Millenium 32 software package (Waters). TLC analyses were performed on silica gel 60 F_{254} plates (Merck), and visualization of plates was carried out using a $Ce_2(SO_4)_3$ (10%) solution in H_2SO_4.

Fungal Material. The fungus was isolated from a soil collected in a cave in Juxtlahuaca (17°25′36″ N, 99°7′34″ W), State of Guerrero, Mexico, in 1998. A reference sample (MEXU 26014) of the isolate was deposited at the Herbario Nacional de Mexico (MEXU). Stock cultures of the fungus are stored in potato-dextrose agar (PDA) and monthly subcultured for preservation.

Fermentation, Extraction, and Isolation. The fungus *P. lilacinum* was grown in PDA Petri dishes for 15 days; then the agar was cut into pieces (1 cm^2) and inoculated in six 1.8 L Fernbach flasks, each containing 1.4 L of potato-dextrose broth (PDB). Inoculated flasks were incubated at room temperature for 21 days in static conditions. After incubation, the contents of the flasks were combined and filtered through cheesecloth. The separated mycelium was macerated with a mixture of CH_2Cl_2−MeOH (9:1), and the culture media was subjected to successive partitions with CH_2Cl_2. The mycelia and broth extracts were combined according to their chromatographic homogeneity and evaporated under reduced pressure to afford a yellow, oily extract (980 mg). The total extract was suspended in 400 mL of a mixture of MeCN−MeOH (1:1) and partitioned with *n*-hexane (3 × 350 mL). The combined MeCN−MeOH fractions were dried *in vacuo*, and the resulting residue (350 mg) was dissolved in MeOH and subjected to RP-HPLC separation on a semipreparative Purospher column to yield **1** (115 mg, t_R 26.2 min) and **2** (21 mg, t_R 21.9 min).

Acremoxanthone C: yellow solid; $[\alpha]_D$ +537 (*c* 0.01, $CHCl_3$); UV ($CHCl_3$) λ_{max} (log ε) 244, 371 nm; IR ν_{max} (KBr) 3416, 2956, 1738, 1570, 1221 cm^{-1}; ^{1}H NMR ($CDCl_3$, 500 MHz) δ 14.32 (1H, br s, OH 8′), 14.17 (1H, s, OH 6), 11.41 (1H, s, OH 6′), 11.10 (1H, s, OH 10), 6.88 (1H, d, *J* = 1.3 Hz, H-3′), 6.79 (1H, dd, *J* = 0.5, 1.5 Hz, H-5′), 6.50 (1H, dd, *J* = 2.1, 10.3 Hz, H-4), 6.42 (1H, dd, *J* = 6.6, 8.5 Hz, H-12′), 6.13 (1H, s, H-11), 6.12 (1H, dd, = 2.8, 10.3 Hz, H-5), 6.08 (1H, dd, *J* = 1.1, 8.5 Hz, H-13′), 5.96 (1H, s, H-1′), 5.29 (1H, dd, *J* = 2.3, 2.8 Hz, H-3), 4.80 (1H, dd, *J* = 1.1, 6.6 Hz, H-11′), 3.69 (3H, s, H-16), 3.65 (1H, br s, OH-3), 2.88 (1H, d, *J* = 17.8 Hz, H-15′a), 2.68 (1H, d, *J* = 18.0 Hz, H-15′b), 2.37 (3H, s, H-16′), 1.98 (3H, s, H-18′); ^{13}C NMR ($CDCl_3$, 125 MHz) δ 21.26 (CH_3, C-18′), 22.22 (CH_3, C-16′), 35.30 (CH_2, C-15′), 38.27 (CH, C-11′), 41.63 (C, C-14′), 53.27 (CH_3, C-16), 73.18 (CH, C-1′), 74.76 (CH, C-3), 84.83 (C, C-2), 99.18 (C, C-7), 105.56 (C, C-9), 105.76 (C, C-9′), 112.60 (C, C-7′), 114.36 (CH, C-11), 115.13 (C, C-13), 119.56 (CH, C-5′), 123.43 (CH, C-3′), 123.74 (CH, C-5), 131.91 (CH, C-12′), 132.66 (CH, C-13′), 136.50 (C, C-2′), 143.90 (CH, C-4), 147.73 (C, C-12), 147.91 (C, C-4′), 154.23 (C, C-14), 159.99 (C, C-10), 161.72 (C, C-6′), 168.87 (C, C-15), 170.57 (C, C-17′), 171.19 (C, C-6), 185.23 (C, C-8), 185.60 (C, C-8′), 186.27 (C, C-10′).

Construction of *h*CaM T110C-mBBr Biosensor. Cloning and subcloning were done as previously reported using the pGEM-T Easy Vector System I and vector pET12b with restriction enzymes *NdeI* and *Bam*HI.[20] Amino acid substitutions were generated by overlapping PCR mutagenesis using the Quick Change Kit (Stratagene, La Jolla, CA, USA). The amount of plasmid pET12b-*h*CaM was 100 ng, and the amount of mutagenic oligonucleotides was 125 ng. PCR amplification included 25 cycles of denaturation at 95 °C for 1 min, annealing using a temperature ramp from 45 to 60 °C, a heating rate of 0.2 °C/s, and polymerization at 68 °C for 10 min, followed by one final extension step at 68 °C for 10 min. Oligonucleotides used to generate the single mutant T110C were 5′-CGT CAC GTC ATG TGT AAC TTA GG-3′ and 5′-CCT AAG TTA CAC ATG ACG TGA CG-3′. After the mutagenesis experiments, the products of PCR amplification were digested with *DpnI* enzyme and transformed in DH5α competent cells. The sequence of construction and mutation was confirmed by nucleotide sequencing with an ABI PRISM 310 genetic analyzer (Applied Biosystems, Foster City, CA, USA). Plasmids (pET12b-*h*CaM T110C) were transformed into *E. coli* BL21-AI One Shot following the specifications of the kit's manufacturer.

Protein Purification of the Mutant *h*CaM T110C. A single colony of *E. coli* strain BL21-AI/pET12b-*h*CaM T110C was grown overnight in LB medium containing 100 mg/mL ampicillin with shaking at 37 °C and inoculated into 500 mL of LB medium containing 100 mg/mL ampicillin, until the optical density of the culture at 550 nm reached between 0.8 and 1.0. Expression was induced by the addition of L-(+)-arabinose (0.2% w/v) overnight with shaking at 37 °C. The cells were harvested by centrifugation (10 min, 4000*g*), resuspended in 50 mM Tris-HCl, 2 mM EDTA, 1 mM dithiothreitol (DTT), and 200 mg/mL egg white lysozyme at pH 7.5, and chilled on ice for 30 min. Resuspended cells were lysed by sonication, and cellular debris was removed by centrifugation for 15 min at 15000*g*. The supernatant was collected, and $CaCl_2$ and NaCl were added to final concentrations of 5 and 500 mM, respectively. The protein was purified using a Phenyl Sepharose CL-4B chromatographic column. Briefly, the supernatant was applied to the column pre-equilibrated with 50 mM Tris-HCl, 0.5 mM DTT, 0.1 mM $CaCl_2$, and 500 mM NaCl at pH 7.5. The column was washed with loading buffer followed by the same with 1 mM EDTA and 150 mM NaCl. Finally, the protein was loaded on a cationic exchange column (Source Q, Amersham Biosciences) at pH 8.8 and eluted by a linear gradient of 40 min (0−100%) with 500 mM NaCl. Protein was collected in fractions and assessed for purity by gel electrophoresis.

Chemical Modification of Unique Reactive Cysteine of *h*CaM T110C Protein with *m*BBr. All fluorophore conjugation steps were typically carried out at room temperature. To protein at a concentration of 5−10 mg/mL was added 5 mM DTT by 12 h to reduce intramolecular disulfide bonds; then the mixture was washed on a gel filtration HR-100 column (Pharmacia, Biotech) to eliminate the excess DTT. A thiol-reactive fluorophore (20% in DMSO) was added in small aliquots to reach a final concentration of 10 molar excess and DMSO about 5%. Conjugation proceeded in the dark overnight at 4 °C with shaking. Separation of protein from unreacted fluorophore was achieved by size-exclusion chromatography (Superdex 75). The efficiency of report group attachment was assessed by the reactivity of the protein against 5,5′-dithiobis(2-nitrobenzoic) acid, measuring the release of 2-nitrobenzoate. Next, protein concentration of labeled *h*CaM was determined with the bicinchoninic acid method.[32]

Steady-State Fluorescence Bioassay (*h*CaM M124C-*mBBr* and *h*CaM T110C-*mBBr* biosensors). All measurements were conducted with an ISS-PC1 spectrofluorometer (ISS, Champaign, IL, USA) with sample stirring at 37 °C. The fluorescent biosensors *h*CaM M124C-*mBBr* and *h*CaM T110C-*mBBr* (1 mM), obtained as previously described,[20] were incubated in the buffer (50 mM NaOAc [pH 5.1] and 10 nM $CaCl_2$); then, after 5 min the ligand dissolved in MeOH (10 nM) was added. Fluorescence emission spectra were acquired with excitation and emission slit widths of 4 and 8 nm, respectively. The excitation wavelength was 381 nm, and emission wavelengths were measured in a range of 415−550 nm. The fractional saturation (y) of the *h*CaM M124C-*mBBr*-ligand and *h*CaM T110-*mBBr*-ligand complexes was calculated by changes in fluorescence upon ligand binding according to $y = (F - F_0)/(F_\infty - F_0)$, where F_∞ represents the fluorescence intensity at full saturation with the ligand, and y is plotted as a function of the Ca^{2+}−CaM/inhibitor (L); the apparent dissociation constant (K_d) and stoichiometry (S) were obtained by fitting of the equation

$$y = \frac{(1 + K_d/S + L/S) - \sqrt{(1 + K_d/S + L/S)^2 - 4L/S}}{2}$$

where y represents the fractional degree of fluorescence intensity at 470 nm, K_d is the apparent dissociation constant for the ligands, L is the complex−ligand relation, and S is the stoichiometry. Data were analyzed using Origin software version 8.0 (OriginLab, Northampton, MA, USA).

Molecular Modeling. Minimum energy structures were built using the Spartan'02 software (Wavefunction Inc., Irvine, CA, USA). Conformational searching for the different isomers was performed using the Monte Carlo protocol as implemented in the same software, under an MMFF94 molecular mechanics force field. The searching process was repeated at least twice, taking as starting point different geometries in order to achieve a wide range of conformational states. The resulting conformers were filtered according to their energies, leaving all duplicates out. In order to have a wide window of conformers in the Boltzmann distribution, an energy cutoff of 3 kcal/mol was selected. All conformers were geometrically optimized using DFT at the B3LYP/DGDZVP level of theory employing the Gaussian 09 program (Gaussian Inc., Wallingford, CT, USA). The optimized structures were used to calculate the thermochemical parameters and frequencies at 1 atm and 298 K. Magnetic shielding tensors were calculated with the gauge invariant atomic orbital method (GIAO), and coupling constants ($^1H-^1H$, and $^{13}C-^1H$) were obtained from the B3LYP/DGDZVP-optimized structures using the spin−spin option during the NMR calculations. The studies for determining theoretical optical rotation values were achieved at the same level of theory. Both properties were Boltzmann-weighted taking into account the DFT conformational population. All calculations were carried out on the KanBalam cluster, a parallel supercomputer with Linux operating system of distributed memory, containing 1368 AMD Opteron processors, around 3 terabytes of RAM memory, and 160 terabytes of storage (http://www.super.unam.mx/).

Docking Studies. The docking studies were carried out with the AutoDock 4.2 program (http://www.autodock.scripps.edu/). The crystallographic structures of CaM were obtained from the Protein Data Bank (RCSB; pdb codes 1A29, 1XA5). Addition of polar hydrogen atoms, Kollman charges, and solvation parameters to the protein was performed through the AutoDock Tools 1.5.4 package (ADT, http://mgltools.scripps.edu/). Fully optimized structures of the ligands by DFT were taken as starting geometries and prepared by assigning the Gasteiger−Marsilli atomic charges and nonpolar hydrogens using AutoDockTools 1.5.4. Docking was achieved using the default parameters as implemented in the software, except for the number of runs (1000), and the Lamarckian genetic algorithm (LGA) with local search and 25 000 000 energy evaluations per run. Initially a blind docking was conducted with grid box size set at 120 Å × 110 Å × 110 Å in the x, y, and z dimensions, with the protein as the center of the grid. A refinement procedure (grid box set to 60 Å × 60 Å × 60 Å) with the center of the grid corresponding to the ligand at the pose with the least energy obtained in the blind docking was performed. The obtained docked poses were analyzed with AutoDockTools[26,33] using cluster analysis, PyMOL, and LigPlot.[34]

■ ASSOCIATED CONTENT

Ⓢ Supporting Information

DFT B3LYP/DGDZVP free energies, populations, theoretical averaged optical rotations, and theoretical averaged coupling constants for **A**−**H**. ^1H, ^{13}C, and proton-coupled ^{13}C spectra of compound **1**. This material is available free of charge via the Internet at http://pubs.acs.org.

■ AUTHOR INFORMATION

Corresponding Author

*(R.M.) Tel: 525-556225289. Fax: 525-556225329. E-mail: rachel@unam.mx. (C.M.C.-G.-R.) Tel: 525-557474035. E-mail: ccerda@cinvestav.mx.

Notes

The authors declare no competing financial interest.

■ ACKNOWLEDGMENTS

This work was supported by a grant from CONACyT (99395). We thank G. Duarte, M. Guzmán, M. Gutiérrez, I. Rivero, and A. Pérez for their valuable technical assistance. A.M.-M. acknowledges a fellowship from CONACyT to pursue graduate studies. We are indebted to Dirección General de Servicios de Cómputo Académico (DGSCA), UNAM, for providing the

resources to carry out computational calculations through the KanBalam system.

REFERENCES

(1) Luangsa-ard, J.; Houbraken, J.; van Doorn, T.; Hong, S.-B.; Borman, A. M.; Hywel-Jones, N. L.; Samson, R. A. *FEMS Microbiol. Lett.* **2011**, *321*, 141−149.
(2) Oclarit, E. L.; Cumagun, C. J. R. *J. Plant Protein Res.* **2010**, *49*, 337−340.
(3) Demirci, F.; Denizhan, E. *Phytoparasitica* **2010**, *38*, 125−132.
(4) Kiewnick, S.; Sikora, R. A. *Biol. Control* **2006**, *38*, 179−187.
(5) Mikami, Y.; Yazawa, K.; Fukushima, K.; Arai, T.; Udagawa, S.; Samson, R. A. *Mycopathologia* **1989**, *108*, 195−199.
(6) Khan, A.; Williams, K.; Nevalainen, H. *FEMS Microbiol. Lett.* **2003**, *227*, 107−111.
(7) Teles, A. P. C.; Takahashi, J. A. *Microbiol. Res.* **2012**, 1−7.
(8) Rivero-Cruz, J. F.; Macías, M.; Cerda-García-Rojas, C. M.; Mata, R. *J. Nat. Prod.* **2003**, *66*, 511−514.
(9) Rivero-Cruz, B.; Rivero-Cruz, I.; Rodríguez-Sotres, R.; Mata, R. *Phytochemistry* **2007**, *68*, 1147−1155.
(10) Martínez-Luis, S.; Rodríguez, R.; Acevedo, L.; González, M. C.; Lira-Rocha, A.; Mata, R. *Tetrahedron* **2006**, *62*, 1817−1822.
(11) Figueroa, M.; González, M. D. C.; Rodríguez-Sotres, R.; Sosa-Peinado, A.; González-Andrade, M.; Cerda-García-Rojas, C. M.; Mata, R. *Bioorg. Med. Chem.* **2009**, *17*, 2167−2174.
(12) Leyte-Lugo, M.; González-Andrade, M.; González, M. D. C.; Glenn, A. E.; Cerda-García-Rojas, C. M.; Mata, R. *J. Nat. Prod.* **2012**, *75*, 1571−1577.
(13) Ayers, S.; Graf, T. N.; Adcock, A. F.; Kroll, D. J.; Shen, Q.; Swanson, S. M.; Matthew, S.; Carcache de Blanco, E. J.; Wani, M. C.; Darveaux, B. A.; Pearce, C. J.; Oberlies, N. H. *J. Antibiot.* **2011**, *65*, 3−8.
(14) He, H.; Bigelis, R.; Solum, E. H.; Greenstein, M.; Carter, G. T. *J. Antibiot.* **2003**, *56*, 923−930.
(15) Junker, J. P.; Rief, M. *Proc. Natl. Acad. Sci. U.S.A.* **2009**, *106*, 14361−14366.
(16) Yosef, E.; Politi, R.; Choi, M. H.; Shifman, J. M. *J. Mol. Biol.* **2009**, *385*, 1470−1480.
(17) Yurimoto, S.; Hatano, N.; Tsuchiya, M.; Kato, K.; Fujimoto, T.; Masaki, T.; Kobayashi, R.; Tokumitsu, H. *Biochemistry* **2009**, *48*, 3946−3955.
(18) Menyhard, D. K.; Keseru, G. M.; Náray-Szabó, G. *Curr. Comput.-Aided Drug* **2009**, *5*, 264−279.
(19) Horvath, I. *J. Biol. Chem.* **2004**, *280*, 8266−8274.
(20) González-Andrade, M.; Figueroa, M.; Rodríguez-Sotres, R.; Mata, R.; Sosa-Peinado, A. *Anal. Biochem.* **2009**, *387*, 64−70.
(21) Stephens, P. J.; Pan, J. J.; Devlin, F. J.; Cheeseman, J. R. *J. Nat. Prod.* **2008**, *71*, 285−288.
(22) López-Vallejo, F.; Fragoso-Serrano, M.; Suárez-Ortiz, G. A.; Hernández-Rojas, A. C.; Cerda-García-Rojas, C. M.; Pereda-Miranda, R. *J. Org. Chem.* **2011**, *76*, 6057−6066.
(23) Tabata, N.; Tomoda, H.; Matsuzaki, K.; Omura, S. *J. Am. Chem. Soc.* **1993**, *115*, 8558−8564.
(24) Tabata, N.; Tomoda, H.; Iwai, Y.; Omura, S. *J. Antibiot.* **1996**, *49*, 267−271.
(25) Isaka, M.; Palasarn, S.; Auncharoen, P.; Komwijit, S.; Jones, E. B. G. *Tetrahedron Lett.* **2009**, *50*, 284−287.
(26) Morris, G. M.; Goodsell, D. S.; Halliday, R. S.; Huey, R.; Hart, W. E.; Belew, R. K.; Olson, A. J. *J. Comput. Chem.* **1998**, *19*, 1639−1662.
(27) Harmat, V.; Böcskei, Z.; Náray-Szabó, G.; Bata, I.; Csutor, A. S.; Hermecz, I.; Arányi, P.; Szabó, B.; Liliom, K.; Vertessy, B. G.; Ovádi, J. *J. Mol. Biol.* **2000**, *297*, 747−755.
(28) Lakowicz, J. R. *Principles of Fluorescence Spectroscopy*; Springer: New York, 2006; p 86.
(29) Martínez-Luis, S.; Pérez-Vásquez, A.; Mata, R. *Phytochemistry* **2007**, *68*, 1882−1903.
(30) Figueroa, M.; González-Andrade, M.; Sosa-Peinado, A.; Madariaga-Mazon, A.; Del Río-Portilla, F.; González, M. D. C.; Mata, R. *J. Enzyme Inhib. Med. Chem.* **2011**, *26*, 378−385.
(31) González-Andrade, M.; Rivera-Chávez, J.; Sosa-Peinado, A.; Figueroa, M.; Rodríguez-Sotres, R.; Mata, R. *J. Med. Chem.* **2011**, *54*, 3875−3884.
(32) Smith, P. K.; Krohn, R. I.; Hermanson, G. T.; Mallia, A. K.; Gartner, F. H.; Provenzano, M. D.; Fujimoto, E. K.; Goeke, N. M.; Olson, B. J.; Klenk, D. C. *Anal. Biochem.* **1985**, *150*, 76−85.
(33) Huey, R.; Morris, G. M.; Olson, A. J.; Goodsell, D. S. *J. Comput. Chem.* **2007**, *28*, 1145−1152.
(34) Wallace, A. C.; Laskowski, R. A.; Thornton, J. M. *Protein Eng.* **1995**, *8*, 127−134.
(35) This paper is taken in part from the Ph.D. thesis of A.M.